

A Fully Lagrangian Advection Scheme

John C. Bowman · Mohammad Ali
Yassaei · Anup Basu

October 2, 2014

Abstract A numerical method for passive scalar and self-advection dynamics, *Lagrangian rearrangement*, is proposed. This fully Lagrangian advection algorithm introduces no artificial numerical dissipation or interpolation of parcel values. In the zero-viscosity limit, it preserves all of the Casimir invariants associated with parcel rearrangement. In the two-dimensional case presented here, these invariants are arbitrary piecewise continuous functions of the vorticity and concentration fields. The initial parcel centroids are evolved in a Lagrangian frame, using the method of characteristics. At any time this Lagrangian solution may be viewed by projecting it onto an Eulerian grid using a rearrangement map. The resulting rearrangement of initial parcel values is accomplished with a weighted Bresenham algorithm, which identifies quasi-optimal, distributed paths along which chains of parcels are pushed to fill in nearby empty cells. The error introduced by this rearrangement does not propagate to future time steps.

Keywords incompressible viscous fluids · Lagrangian advection · Casimir invariants · parcel rearrangement · relabelling symmetry

Mathematics Subject Classification (2010) 76M25 · 76D99 · 76M27

This work was supported by the Natural Sciences and Engineering Council (NSERC) of Canada.

J. Bowman

Tel.: +1-780-492-0532 Fax: +1-780-492-6826 Department of Mathematical and Statistical Sciences, University of Alberta, Edmonton, Alberta T6G 2G1, Canada E-mail: bowman@ualberta.ca

M. Yassaei

Department of Mathematical and Statistical Sciences, University of Alberta, Edmonton, Alberta T6G 2G1, Canada E-mail: m.a.yassaei@gmail.com

A. Basu

Department of Computing Science, University of Alberta, Edmonton, Alberta T6G 2E8, Canada E-mail: basu@ualberta.ca

1 Introduction

The advection–diffusion equation arises in many scientific disciplines such as electro-osmotic flow, geophysical fluid dynamics (including meteorology, climate change, and hurricane prediction), thermonuclear fusion in plasmas, and mathematical biology. A model of electro-osmotic advection characterized by extremely small diffusion rates provided the initial motivation for the development of this work [1,11]. Consider the incompressible advection–diffusion equation

$$\frac{\partial \mathbf{U}}{\partial t} + \mathbf{v} \cdot \nabla \mathbf{U} = \mathbf{D} \nabla^2 \mathbf{U}, \quad (1)$$

where the advecting velocity field $\mathbf{v} = \mathbf{v}(\mathbf{x}, t)$ satisfies the solenoidal condition $\nabla \cdot \mathbf{v} = 0$, and \mathbf{D} is a constant diagonal diffusion matrix. The advecting velocity is either a specified field (*passive advection*) or a functional of \mathbf{U} (*self-advection*). We are primarily interested in the transport of a self-advected quantity $\mathbf{U} = (\omega, C)$ by a two-dimensional fluid that flows in a domain with velocity \mathbf{v} , where the quantities $C = C(\mathbf{x}, t)$ and $\omega \hat{\mathbf{z}} = \boldsymbol{\omega}(\mathbf{x}, t) = \nabla \times \mathbf{v}$ represent the *concentration* and *vorticity* fields, respectively, and $\hat{\mathbf{z}}$ is a unit vector normal to the plane of the flow. When the velocity \mathbf{v} is *incompressible* ($\nabla \cdot \mathbf{v} = 0$), the advection equation is an example of a flux-conservative system $\partial \mathbf{U} / \partial t = -\nabla \cdot \mathbf{F}$, where $\mathbf{F} = \mathbf{v} \mathbf{U} - \mathbf{D} \cdot \nabla \mathbf{U}$. In self-consistent advection, the velocity is typically determined by the incompressible *Navier–Stokes* equation

$$\frac{\partial \mathbf{v}}{\partial t} + \mathbf{v} \cdot \nabla \mathbf{v} = -\frac{1}{\rho} \nabla P + \nu \nabla^2 \mathbf{v}, \quad (2)$$

where $\mathbf{v} = \mathbf{v}(x, t)$ is the velocity, P is the pressure, ρ is the density, and ν is the viscosity. It is convenient to take the curl of (2) to eliminate the pressure field P , which leads to an equation for the vorticity:

$$\frac{\partial \omega}{\partial t} + \mathbf{v} \cdot \nabla \omega = \nu \nabla^2 \omega. \quad (3)$$

The concentration field evolves according to

$$\frac{\partial C}{\partial t} + \mathbf{v} \cdot \nabla C = \mathbf{D} \nabla^2 C, \quad (4)$$

where D is a scalar diffusion constant, so that $\mathbf{D} = \begin{pmatrix} \nu & 0 \\ 0 & D \end{pmatrix}$ in (1).

The general solution of the passive advection equation with no diffusion,

$$\frac{\partial C}{\partial t} + \mathbf{v} \cdot \nabla C = 0, \quad (5)$$

is a wave moving with velocity \mathbf{v} . This solution $C(\mathbf{x}, t) = C(\boldsymbol{\xi}_0(\mathbf{x}, t), 0)$ can be written in terms of the *initial parcel position* $\boldsymbol{\xi}_0 = \boldsymbol{\xi}_0(\mathbf{x}, t)$ defined by the Lagrangian position variable $\boldsymbol{\xi}(t) = \boldsymbol{\xi}_0 + \int_0^t \mathbf{v}(\boldsymbol{\xi}(\tau), \tau) d\tau$ such that $\boldsymbol{\xi}(t) = \mathbf{x}$.

In the special case where the velocity field $\mathbf{v} = \mathbf{v}(\tau)$ is independent of position, $\boldsymbol{\xi}_0(\mathbf{x}, t) = \mathbf{x} - \int_0^t \mathbf{v}(\tau) d\tau$ and $C(\mathbf{x}, t) = C\left(\mathbf{x} - \int_0^t \mathbf{v}(\tau) d\tau, 0\right)$.

It is well known that the forward-time centered-space Eulerian differencing scheme for advection is unstable (e.g., see [31]). Conventional methods for avoiding this instability sacrifice accuracy. For example, the *Lax scheme* adds a diffusion term, or *numerical dissipation*, to the partial differential equation. This method is stable if the time step is chosen to satisfy the *Courant condition* [10]. To help counter the effect of numerical dissipation, one can use *flux-corrected transport*, which adds an *anti-diffusion* term to the equation [41, 36]. *Upwind differencing* is a stable discretization that accounts for the fact that the rate of change of the flow is directionally dependent, but it adds unwanted numerical dissipation and is only first-order accurate in the time step. The *staggered leapfrog* method is a centered-time centered-space discretization based on two staggered temporal partitions. It is second-order accurate in time, as is the *two-step Lax–Wendroff* scheme [24], in which the flux is calculated and used to determine the concentration field at the next time step.

Lagrangian schemes use a grid that moves with the flow as opposed to an Eulerian fixed grid. That is, derivatives are calculated in the Lagrangian frame of reference, where advection is most naturally described. In this frame the variable \mathbf{x} is also a function of t and, in the absence of dissipation, the *total derivative* of C is zero:

$$\frac{dC(\mathbf{x}(t), t)}{dt} = \frac{d\mathbf{x}}{dt} \cdot \nabla C + \frac{\partial C}{\partial t} = \mathbf{v} \cdot \nabla C + \frac{\partial C}{\partial t} = 0,$$

where $\mathbf{v} = d\mathbf{x}/dt$. This conservation equation expresses the fact that the scalar field C is neither created nor destroyed, only rearranged, by the advecting field \mathbf{v} . The two key components of any Lagrangian scheme are: (i) a method for following the characteristics; and (ii) a method for viewing the solution on an Eulerian grid. In *fully Lagrangian schemes*, the grid is attached to and moves with the flow. In conventional implementations of Lagrangian schemes, one typically needs to remesh after a finite number of time steps. In this work, we propose a fully Lagrangian scheme that does not require remeshing. The characteristics of the flow are followed using the classical fourth-order Runge–Kutta algorithm. The centroids of a finite number of discrete parcels characterized by distinct values of $\boldsymbol{\xi}_0$ are evolved on a spatial grid. At each time step, the new position of a given parcel is computed using its previous position and the local flow velocity.

To view a fully Lagrangian solution to an advection problem on an Eulerian grid, one also needs a projection scheme. Normally, area-weighted interpolation is used. However, in this work we construct a scheme for projecting onto the rearrangement manifold that respects an infinite hierarchy of conservation laws essential to a proper mathematical model of advection. Even when diffusion is added to this fully Lagrangian algorithm (using a semi-Lagrangian area-weighted interpolation scheme like the one described next), our proposed algorithm (illustrated in Fig. 5) exhibits much better energy decay characteristics (cf. Fig. 14).

In *semi-Lagrangian schemes*, the grid is fixed in time: although the advective derivatives are calculated in a Lagrangian frame, the other spatial derivatives are calculated on an Eulerian grid. The idea is to discretize the advective terms in a Lagrangian frame and then project the Lagrangian solution back onto an Eulerian grid, avoiding the instability of forward-time-centered-space Eulerian schemes and the inherent complications of fully Lagrangian remeshing. For example, in the advection scheme for shallow water waves described by Behrens [5], backtracked trajectories seldom land on a grid point. Interpolation is therefore used in order to determine the values of C between grid points. This interpolation can produce large numerical dissipation. Moreover, it does not respect fundamental properties of the flow, specifically the conservation of the Casimir invariants discussed in the next section. In problems involving a mass flow, it is sometimes possible to modify a semi-Lagrangian scheme so that it at least conserves mass (for example, see [4] and [26]).

The *particle-in-cell* method represents a piecewise constant approximation of the solution as a mesh of moving nodes (“particles”) advected by the flow. First, the positions of the particles are advected in the Lagrangian frame. Their associated physical attributes (in our case vorticity and concentration values) are then projected using area-weighted interpolation onto a finite Eulerian grid. One can then solve for the contributions to the evolution from diffusion and any other nonadvective terms on the Eulerian grid and project the result back onto the Lagrangian grid, again using area-weighted interpolation. The procedure is then repeated for the next time step (for example, see [25] and [20]). Particle-in-cell methods tend to be noisy unless a very large number of particles are used. While they guarantee mass conservation, other conservation laws, such as energy conservation, are not necessarily guaranteed. A variation of the particle-in-cell approach, smoothed particle hydrodynamics [17,34], adjusts the particle characteristic size and/or shape to local conditions, allowing the resolution of the simulation to automatically adapt to inhomogeneities in the flow, without the complications and expense of constructing a dynamically adaptive grid.

Godunov [18] developed a discretization for fluid dynamics with shocks by modelling the fluid as a large number of uniform cells joined by the *Riemann solution* for the dynamics at an interface between two uniform fluid regions. For example, L. Fraccarollo, H. Capart, and Y. Zech [16] developed a finite-volume solver by using the Godunov method to estimate the flux from the solution to the Riemann problem for open-channel flows. A higher-order extension of the Godunov method called the *piecewise parabolic method* was presented by Woodward and Colella [38]; it uses high-order spatial interpolation to represent steep discontinuities. In that work, the addition of diffusion is essential. They also performed a comparison between numerical methods for simulating hydrodynamic flow in two dimensions, concentrating on fluid flow with strong shocks [37]. Another class of discretizations suitable for flows with shocks are the *discontinuous Galerkin* finite-element methods, which project the solution onto a basis of discontinuous piecewise polynomial functions.

Level-set methods [29, 19, 27, 23, 33] provide another approach to the advection problem. They use the Hamilton–Jacobi methodology to describe propagating fronts as the zero level set of a higher dimensional function. However, when applied to incompressible flow, level set methods do not automatically conserve area. The related method of contour dynamics [40] describes the evolution of vorticity contours in inviscid two-dimensional flow. Contour surgery [12, 13] provides a topological mechanism for reconnecting contour lines to smooth out the singularities that arise when level sets become highly distorted by the flow.

Wang, Skamarock, and Feingold [35] recently studied the application of advection in weather research and forecasting. They showed that incorporating a positive-definite flux limiter results in fewer cloud droplets and smaller cloud albedo than existing methods. Zhuang, Liu, Anh, and Turner [42] use implicit and explicit Euler approximations to solve the fractional advection–diffusion equation on a finite domain with a nonlinear source term. They propose a fractional method of lines, an extrapolation method, and a matrix transfer technique in the process of solving the problem. Yong, Benson, Meerschaert, and Scheffler [39] use the concept of random-walk particle tracking to solve the space-fractional advection–dispersion equation. While their approach does not require spatial discretization and does not suffer from numerical dispersion, their algorithm handles only the one-dimensional case. A method for solving the advection of large-scale weak magnetic fields in accretion disks was proposed by Rothstein and Lovelace [32]. Their research can be applied to model jet formation; however, limited numerical experiments and verification of their approach were presented.

In this work, a new numerical method for advection that avoids introducing artificial dissipation or the need to remesh, is proposed. In particular, we construct a numerical algorithm that conserves the global (integrated) value of an arbitrary smooth function of C in the limit of zero dissipation. For such systems, future values of the flow quantities are simply rearrangements of the current values. We constrain the numerical discretization to enforce this property by tracking the centroids of discrete parcels from their initial positions forward in time. At any time, the solution may be viewed by projecting it onto a *rearrangement manifold*, the set consisting of all rearrangements of the initial conditions. In Section 2 we introduce a method to conserve the Casimirs invariants, and the algorithm for this method is discussed in Section 3. The complexity of the algorithm is approximated in Section 5. We extend the algorithm to handle both diffusion and self-consistent advection in Section 4. Finally, in Section 6 the method is illustrated numerically and compared with a conventional semi-implicit scheme.

2 Lagrangian rearrangement

In this section we propose the method of *Lagrangian rearrangement* for projecting a fully Lagrangian solution of the passive advection equation, (5), onto

an Eulerian grid. We first illustrate the method in the absence of diffusion. We constrain the numerical discretization to mimic an important analytic property of advection, namely, the conservation of the global integral of any smooth C^1 function of the scalar concentration field:

$$\begin{aligned} \frac{d}{dt} \int f(C) d\mathbf{x} &= \int f'(C) \frac{\partial C}{\partial t} d\mathbf{x} = - \int f'(C) \mathbf{v} \cdot \nabla C d\mathbf{x} \\ &= - \int \mathbf{v} \cdot \nabla f(C) d\mathbf{x} = \int f(C) \nabla \cdot \mathbf{v} d\mathbf{x} = 0, \end{aligned} \quad (6)$$

using the incompressibility of the advecting velocity field \mathbf{v} . Note that the above equation also holds in the self-advected case when C is replaced by ω , which depends on the advecting velocity \mathbf{v} , so that $\frac{d}{dt} \int f(\omega) d\mathbf{x} = 0$. Equation (6) expresses the conservation of uncountably many *Casimir invariants* (e.g., see [28]). It also holds when f is piecewise constant, where we interpret f' as a distribution.

If we take f to be unity for a specified range of C values and zero elsewhere, we see that the area of the flow associated with that range of C values must be invariant. Since connectedness is preserved by the continuous (and area-preserving) advection map, we deduce that a connected parcel having a particular C range gets mapped to a connected parcel of the same area. Moreover, if the C values are partitioned into n uniform ranges, the evolved state will consist of n distinct nonoverlapping patches associated with these ranges, possibly highly distorted. Therefore, assuming that C is initially bounded, as n goes to infinity, the resulting infinitesimal patches become rearranged into a highly complicated but nonoverlapping union of distorted parcels. Values of C that were not present in the initial configuration cannot be created, nor can existing C values be destroyed. Motivated by this exact property of infinitesimal parcel rearrangement, in the discrete case, we represent the solution $C(\mathbf{x})$ as a piecewise-constant function that takes on the values $C_{i,j}$ in each cell indexed by (i, j) . Under this assumption, the continuum property (6) reduces to

$$\frac{d}{dt} \sum_{i,j} f(C_{i,j}) = 0. \quad (7)$$

We propose that a mathematically faithful numerical model of advection should enforce this discrete version of the above exact infinitesimal property.

On taking $f(C)$ to be 1 if $C = C_0$ for some fixed value C_0 , and zero otherwise, we see that the number of cells with value C_0 would then be invariant, just as in the infinitesimal case. That is, the new values of C at the current time step are prescribed to be rearrangements of the old values (and hence of the initial conditions) at the previous time step. This rearrangement property, depicted in Fig. 1, is known in the literature as a *relabelling symmetry*. If C is assumed to be piecewise continuous, then $f(C)$ is certainly integrable and hence the Darboux integrability theorem guarantees that $\sum_{i,j} f(C_{i,j})$ on a sequence of uniform $N \times N$ grids converges to $\int f(C) d\mathbf{x}$ as $N \rightarrow \infty$. Hence, the value of the latter integral, like the sum, must be constant. We

thus see that (7), if it holds for all discrete grids, is a sufficient condition for the exact property (6) to hold.

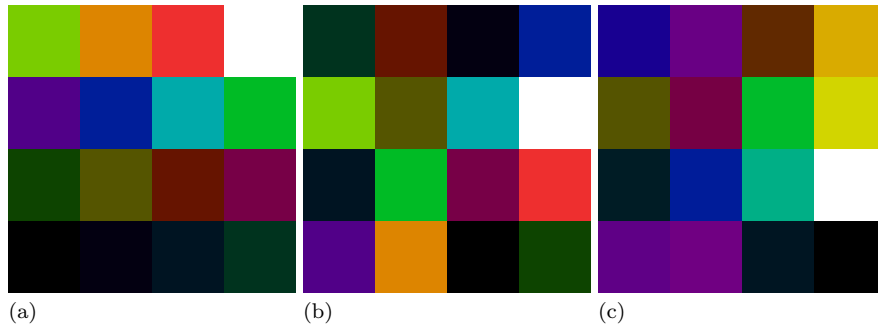


Fig. 1 Demonstration of the parcel rearrangement property of advection in the absence of diffusion. In (a) the initial state consists of a 4×4 Eulerian grid of distinct parcels characterized by different colours. The future state predicted by: (b) Lagrangian rearrangement preserves the initial colours; (c) conventional semi-Lagrangian interpolation mixes the colours, introducing new values and removing others.

The role of Casimir invariants in two-dimensional phenomenological descriptions of fluid flow is unclear. While the energy and enstrophy invariants are known to cascade to the large scales and small scales, respectively, the cascade direction, if any, of the Casimir invariants is controversial. Polyakov's minimal conformal field theory model [30] predicts that higher-order Casimir invariants cascade to large scales, while Falkovich [15] and Eyink [14] argue that they should instead cascade to small scales. Recently, Bowman studied the cascade direction of the global integral of the fourth power of the vorticity numerically with a modified pseudospectral code [6]. While the numerical evidence suggested that this positive-definite Casimir invariant cascades to small scales, the study was complicated by the fact that such higher-order Casimir invariants do not survive wavenumber truncation.

In this work we are therefore motivated to consider an alternative method for discretizing advection equations that builds in the conservation of Casimir invariants from the outset. In order to make contact with the pseudospectral method, we consider a two-dimensional doubly periodic grid of cells. This allows us to focus on the implementation of the parcel rearrangement constraint without being distracted by the additional complications associated with fixed or even moving boundaries.

Each Eulerian cell is initially assigned a parcel of fluid that will be advected in the Lagrangian frame. The *displacement* $\boldsymbol{\xi} = \boldsymbol{\xi}_0 + \int_0^\tau \mathbf{v} dt$ of each parcel is calculated at time τ , where $\mathbf{v} = \mathbf{v}(\boldsymbol{\xi}, t)$ is the local velocity of the flow and $\boldsymbol{\xi}_0$ is the initial displacement. In this fully Lagrangian formulation, the displacement is effectively calculated directly from the initial position, so that projection errors do not propagate to future time steps: the Lagrangian to Eulerian projection onto the rearrangement manifold is used only for viewing

the current state of the fluid, not for actually evolving the fluid. To evaluate the time integral, it is convenient to express the evolution of $\boldsymbol{\xi}$ as the initial value problem $d\boldsymbol{\xi}/dt = \mathbf{v}(\boldsymbol{\xi}, t)$, where $\boldsymbol{\xi}(0) = \boldsymbol{\xi}_0$, for a specified function $\mathbf{v}(\boldsymbol{\xi}, t)$. In the *advection step*, the classical fourth-order Runge–Kutta scheme is used to calculate the current Lagrangian displacement of each parcel. No projection to the Eulerian frame is done here; the Lagrangian position of the parcel is retained to initialize future advection steps.

In classical Lagrangian codes for advection by an incompressible flow, the vertices of the initially square parcels are advected by an area-preserving map to form an irregular Lagrangian mesh consisting of quadrilateral cells. To view the Lagrangian solution, one normally uses area-weighted interpolation to project the contributions from the quadrilaterals onto Eulerian cells. However, in this work we propose that the centroids of these quadrilateral parcels should be mapped onto the rearrangement manifold. Given a fixed velocity field, the above integration at each stage amounts to a linear transformation of the quadrilateral region. Under this transformation, the centroid of a parcel thus maps to the centroid of the new quadrilateral formed by the evolved vertices. For the case of passive advection without diffusion, one does not need to know the actual quadrilateral vertices and instead advects only their centroids.

3 The rearrangement algorithm

Whenever we wish to view the current Lagrangian solution, we project a copy of it onto the rearrangement manifold (i.e., onto the Eulerian grid). For each parcel, we first determine the cell in which its current Lagrangian position lies. The problem that immediately arises is that a given cell may contain more than one such parcel; some sort of competition must then be held to determine which parcel should be projected to that cell. Recall that the discrete rearrangement condition underlying (7) requires that each parcel be mapped to a unique cell. Each cell would then adopt, at that instant, the fluid quantities of its associated parcel.

If the grid has n cells, we will have exactly n parcels. If each parcel lies within a distinct cell, there will be exactly one parcel per cell and we are done. However, in general, there may be some cells denoted as “holes” that do not have any associated parcels and some cells denoted as “piles” that contain more than one parcel. To enforce the preservation of the Casimir invariants during parcel rearrangement, only one parcel from a pile can be transferred to a hole; the others must be moved elsewhere. This step is denoted as the *rearrangement step*. By simply taking the extra parcels in a pile and transferring them to the nearest holes, we would create a discontinuity in the flow, which would constitute an enormous numerical defect. To resolve this issue, we propose the following *pushing algorithm*. This algorithm must not be confused with the so-called “particle-pushing” schemes used to follow the characteristics of the advecting flow. At this point, the advection step has been completed and we

are now dealing with the problem of rearranging the n parcels into n cells for viewing the internal fully Lagrangian solution.

First, we must deal with the issue of treating all of the cells on an equal footing, without giving some the advantage of being processed first. At each stage of the Runge–Kutta advection step, we advect all parcels simultaneously, using the current local velocity, without reference to the locations of any other parcel. However, in the rearrangement step we cannot deal with all piles simultaneously—we must start from one particular cell. In the algorithm below, we start from the piles containing the greatest number of parcels since these are the most difficult cases to resolve. While building the list of such cells, we alternate between putting cells in the front or the back of the list. Refinements that effectively introduce further randomization, to avoid undue bias in our processing decisions, will be discussed in Section 3.2. Our rearrangement algorithm proceeds as follows:

1. Sort the piles by the number of parcels they contain.
2. Start with the piles containing the greatest number n of parcels. Process these cells first.
3. For each such pile (the *starting cell*), define its *first shell* to be the eight cells adjacent to it and *shell* n to be those cells that are adjacent to, but not contained in, shell $n - 1$. Search these rectangular *shells* successively for a hole, beginning with the innermost shell and moving outwards. If more than one hole is found on a shell, choose the one closest to the starting cell in the sense of having minimal *path weight*, as described in Section 3.2.
4. Form the discretized path from the starting cell towards the selected hole.
5. Attach the extra parcel in the starting cell to the first cell along this path, pushing parcels successively along this path until the selected hole is filled with a parcel belonging to the last cell along the path. The second cell in the path will thus take the extra parcel in the starting cell, and the next cell will take the parcel previously located in the second cell, and so on. Continue this pushing until the selected hole has been assigned a parcel, or in other words, an initial value. The starting cell now has $n - 1$ parcels in it.
6. Proceed with the next pile containing n parcels, and repeat Steps 3–5 until no more cells containing n parcels remain.
7. Repeat Steps 2–6 until all cells contain exactly one parcel; that is, until $n = 1$.

Notice that after Step 5, all cells along the path will have a new parcel in them relative to their status at the end of the advection step. The corresponding hole is filled with one parcel, and the starting cell will have one less parcel in it than it had before. At the end of Step 7, all cells will contain exactly one parcel, as desired. The rearrangement step is then complete, and each cell can have a unique value assigned to it. For example, since parcels E and F in Fig. 2 belong to a pile, the nearest hole and a discretized path to it are found for the parcel F . It is pushed to the first cell in the path, pushing the next

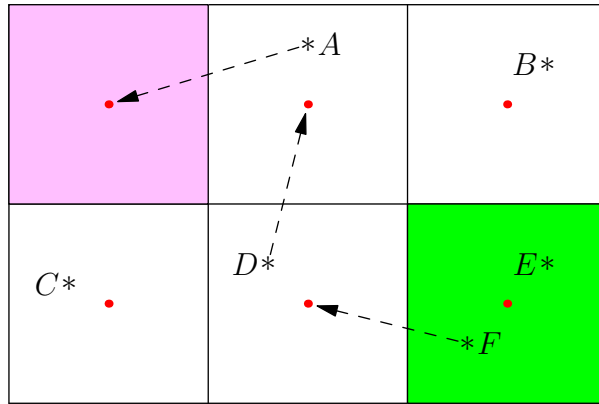


Fig. 2 Rearrangement step: parcels, denoted by stars, are pushed from the pile (green cell) to the hole (pink cell). Dots denote cell centers and arrows indicate parcel pushing.

parcel, D , to the next cell in the path and ultimately putting parcel A into the hole.

3.1 Parcel weights

A straightforward application of Bresenham's algorithm [9] to select a (discretized) path between a pile and a hole can increase the possibility of a parcel being pushed multiple times. Suppose that in one time step, there are clusters of piles concentrated in one area and a group of holes in another nearby area. In pushing a parcel from a pile to a hole, each parcel in between is pushed once. If we process another parcel from the same crowded pile area and push toward the same hole area, the parcels in between may be pushed a second time. Processing all the parcels in this area can cause multiple pushes for parcels in between the pile-rich and hole-rich areas that can result in spurious streaks in the flow visualization. We can avoid multiple pushes by choosing a random path from a pile to a hole, introducing stochasticity into the algorithm. Moreover, a parcel may be pushed far away from its original Lagrangian position, resulting in large errors. In order to choose the best path, we introduce a path weight for discretizing the line. Let the *parcel weight* d represent the distance between the Lagrangian position of a parcel and the center of the cell into which it has been pushed. Each time the parcel is pushed, the cell containing it will change, resulting in a change in d (with no change to the Lagrangian position of the parcel). To alter the Bresenham algorithm to a weighted algorithm, we take d into account when calculating the path between a pile and a hole: parcels are inserted in such a way that the one with minimum d will be first in the list, so that it will be processed or pushed first. This ensures that parcels are not pushed too far from their Lagrangian positions.

3.2 A weighted Bresenham algorithm

In the weighted version of the algorithm (Appendix A), the next cell to be included in the path will be the cell containing the parcel with the minimum parcel weight of all parcels in certain eligible neighbouring cells. In each case, to minimize excursions from the Lagrangian (advected) positions, we choose the cell that contains the parcel with minimal distance d from its Lagrangian position. In the rare case when parcels in the selected cells share the same minimal value of d , we will pick the cell that the original Bresenham algorithm would have picked. Depending on the choice of the next cell, we increment the x and/or y coordinate by one, and include the new cell in the path. The problem is thus reduced to a new problem, using the cell just selected as the new starting point. On reaching the hole, the algorithm terminates (see Theorem 1 in Appendix B). Other quadrants are dealt with in the same manner, but the signs of some of the parameters are changed to decrement (rather than increment) the x and/or y coordinates by one.

A question arises in the case where more than one hole is found in the same rectangular shell around the pile: which hole should be selected as the destination? We resolve such cases by invoking the weighted Bresenham algorithm on all possible choices of holes within the shell, without actually pushing any parcels. We define the *path weight* of a particular path to be the sum of all d values of the parcels to be pushed along that particular path. The Bresenham path that returns the minimum path weight and its corresponding hole will be chosen as the desired path and final destination, respectively. The theorem in Appendix B establishes an upper bound, $\lceil 1.82x \rceil$, on the number of steps required by our weighted Bresenham algorithm to draw a line between two grid points on a unit square lattice that are x units apart. This is not much greater than the $\lceil \sqrt{2}x \rceil$ steps required to draw a diagonal Bresenham line on a unit lattice.

4 Extension to self-consistent advection and diffusion

To solve the general advection–diffusion equation,

$$\frac{\partial U}{\partial t} + \mathbf{v} \cdot \nabla U = D \nabla^2 U, \quad (8)$$

we need to add the diffusion term, as well as a method for handling self-advection, to our algorithm. A significant source of error in the rearrangement algorithm used to project the solution to the Eulerian grid for viewing comes from the somewhat arbitrary algorithm used to push parcels from piles to holes. If the rearrangement algorithm were used to solve the diffusion or self-advection terms, errors would accumulate since the pushed values would be reused in calculating diffusion and self-advection. For the self advection of vorticity described by $\partial\omega/\partial t + \mathbf{v} \cdot \nabla\omega = \nu \nabla^2\omega$, the advection term $\mathbf{v} \cdot \nabla\omega$ would use the pushed values of ω to calculate \mathbf{v} , so that errors associated

with pushing parcels would propagate to future time steps. More importantly, the use of the rearranged vorticity field in calculating the diffusion term $\nu\nabla^2\omega$ would introduce large gradients in the flow, resulting in excessive diffusion. To prevent this propagation of error, we calculate the diffusion term as $\nu\nabla^2\omega$, where ω is the vorticity field on an Eulerian grid obtained by an area-weighted interpolation of the Lagrangian vorticity field (it is difficult to calculate a Laplacian directly on a nonuniform Lagrangian grid). This decision does not degrade the desired conservation properties (Casimir invariants) of the advective term. We calculate the advecting velocity $\mathbf{v} = \hat{\mathbf{z}} \times \nabla \nabla^{-2}\omega$ from ω using a Poisson solver. The advecting velocity itself does not need to be a rearrangement of the initial conditions in order to conserve the Casimir invariants. The diffusion of the concentration field C is handled in the same manner.

We now discuss the scheme for transferring information (interpolating) between the Lagrangian and Eulerian grids. The transfer is done by area-weighted bilinear interpolation. Ideally, one should account for parcel distortion by the flow and project the area bounded by the evolved vertices of the parcel (which form a quadrilateral) to the Eulerian grid. However, as the evolved parcel shape is not essential to the demonstration of how Lagrangian rearrangement can be integrated with diffusion and self-advection, for simplicity we treat each parcel as a square centered on its current Lagrangian position (the parcel centroid), in analogy with the fixed particle shape used in particle-in-cell methods. To project information from a Lagrangian frame to an Eulerian lattice, consider the (ω, C) values of the i th parcel, which we denote by $\overline{\mathbf{U}}_i$ (see Fig. 3). This square will overlap some cells in the grid. Let A_{ij} denote the area of the square centered on parcel i that overlaps with cell j . On accounting for the contributions from all parcels whose bounding squares overlap the cell j , the interpolated value \mathbf{U}_j is calculated as $\mathbf{U}_j = \sum_i A_{ij} \overline{\mathbf{U}}_i / \sum_i A_{ij}$. If no parcels contribute to a cell, we search outward in successive rectangular shells around the empty cell for cells that have a contribution from some parcel. The first shell that is found to contain such cells is used to assign a value, namely the area-weighted average value over these nonempty cells, to the empty cell.

To transform information from the Eulerian to the Lagrangian frame, again consider a parcel and its bounding square (see Fig. 4). This square will overlap at most four cells in the grid. For each of the overlapping cells, compute the Lagrangian value for the parcel as $\sum_j A_j \mathbf{U}_j$, where \mathbf{U}_j is the Eulerian value for the j th cell and A_j is the overlapping area with the parcel's bounding square.

The above two procedures are typically used in tandem. For example, to calculate $\nabla^2\omega$ we need to interpolate the Lagrangian values onto the Eulerian grid, where it is convenient to calculate the Laplacian, and then transfer this contribution to the evolution back to the Lagrangian frame. The Laplacian was evaluated using the standard compact five-point stencil.

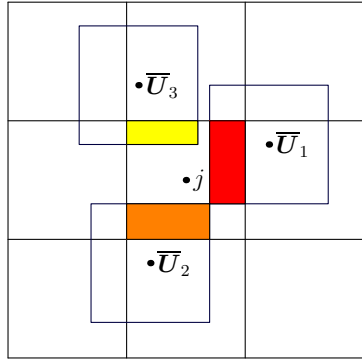


Fig. 3 Projection from a Lagrangian to Eulerian grid.

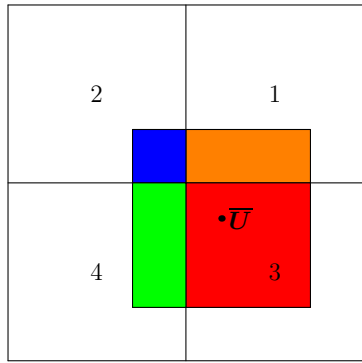


Fig. 4 Projection from an Eulerian to Lagrangian grid.

4.1 Diffusion

In this section we consider the numerical treatment of the diffusion term in (8). The advection term is dealt with using the Lagrangian algorithm discussed in Section 2, and diffusion is handled by a *Crank-Nicholson* scheme (e.g., see [2]) in an Eulerian frame:

$$\frac{\mathbf{U}(t + \tau) - \mathbf{U}(t)}{\tau} = \mathbf{D} \frac{\nabla^2 \mathbf{U}(t + \tau) + \nabla^2 \mathbf{U}(t)}{2}.$$

To incorporate diffusion into our algorithm, it is helpful to split (8) into two pieces, one accounting for advection and the other for diffusion, using *operator splitting* (e.g., see [2]). Let $\tilde{\mathbf{U}}$ be the Eulerian projection of the Lagrangian solution to the advection equation $\partial \tilde{\mathbf{U}} / \partial t = -\mathbf{v} \cdot \nabla \tilde{\mathbf{U}}$ using the area-weighted interpolation (Fig 3). Then, to solve for \mathbf{U} , including the effects of diffusion,

we use the temporal finite-difference formula

$$\frac{\mathbf{U} - \tilde{\mathbf{U}}}{\tau} = \mathbf{D}\nabla^2 \left(\frac{\mathbf{U} + \tilde{\mathbf{U}}}{2} \right). \quad (9)$$

In this formulation, the most up-to-date (i.e., already advected) value, $\tilde{\mathbf{U}}$, is used as the starting value to calculate the diffused value \mathbf{U} . This implicit equation can be rewritten as $\mathcal{L}(-\tau)\mathbf{U} = \mathcal{L}(\tau)\tilde{\mathbf{U}}$, where $\mathcal{L} = \mathbf{1} + \frac{1}{2}\mathbf{D}\tau\nabla^2$. In order to calculate \mathbf{U} numerically, one needs to invert the Helmholtz operator \mathcal{L} . We accomplish this inversion with an efficient *multigrid* solver [21,8], using a single V-cycle iteration and the area-weighted interpolated Eulerian value $\tilde{\mathbf{U}}$ as the initial guess. The multigrid method is an efficient method for solving elliptic equations like the Poisson and Helmholtz equations.

To determine the contribution of diffusion on the Lagrangian solution, we project the difference $\mathbf{U} - \tilde{\mathbf{U}} = [\mathcal{L}^{-1}(-\tau)\mathcal{L}(\tau) - 1]\tilde{\mathbf{U}}$, onto the Lagrangian frame using area-weighted bilinear interpolation (Fig. 4). These Lagrangian contributions are then added onto the parcel values. Note that we do not simply project the diffused solution \mathbf{U} itself onto the Lagrangian frame, as this would contaminate the Lagrangian solution, violating the preservation of the Casimir invariants in the limit of zero diffusion.

4.2 Self-advection

Until now, we have considered only the case of passive advection, where the velocity of the advecting flow is prescribed. In this section, we discuss self-consistent advection (self-advection), where the velocity of the underlying flow is a functional of \mathbf{U} itself. To calculate the velocity \mathbf{v} , it is convenient to adopt the vorticity formulation: using the projected value ω of the vorticity onto the Eulerian grid determined by area-weighted interpolation, one can compute the stream function ψ from $\omega = \nabla^2\psi$. The inversion of the Laplacian, discretized using the standard compact five-point stencil, is done with 5 iterations (except for the very first step, when we used 40 iterations, due to the lack of a good initial guess) of a V-cycle multigrid solver, using the value of the stream function from the previous time step as the initial guess. Once a good approximation to ψ is determined, it is straightforward to calculate the advecting velocity $\mathbf{v} = \hat{\mathbf{z}} \times \nabla\psi$. This velocity is used to evolve both the vorticity and the concentration fields, self-consistently, in the Lagrangian frame.

The entire self-consistent Eulerian–Lagrangian advection–diffusion algorithm is displayed in Fig. 5 and Algorithm 1, in comparison with a conventional semi-Lagrangian scheme. In the red loop, we calculate the new Lagrangian parcel positions $\boldsymbol{\xi}(t) = \boldsymbol{\xi}_0 + \int_0^t \mathbf{v}(\boldsymbol{\xi}(\tau), \tau) d\tau$, increment the time step, and then repeat the procedure. In the pale blue boxes, to account for the effects of the diffusion term, we interpolate $\bar{\mathbf{U}}$ from the Lagrangian to the Eulerian frame using area-weighted interpolation, followed by operator splitting and the Crank–Nicholson method in the Eulerian frame to solve for \mathbf{U} from (9). The

diffused solution $\mathbf{U} = \mathcal{L}^{-1}(-\tau)\mathcal{L}(\tau)\tilde{\mathbf{U}}$ is the conventional semi-Lagrangian solution (orange output). We then project the difference $\mathbf{U} - \tilde{\mathbf{U}}$ in each Eulerian cell back onto the Lagrangian frame, using area-weighted interpolation to accrue the contributions from diffusion onto the parcels overlapping each cell. In the green boxes, we use the area-weighted interpolated value $\tilde{\mathbf{U}}$ to calculate the stream function $\psi = \nabla^{-2}\omega$ and thereby the self-advected velocity $\mathbf{v} = \hat{\mathbf{z}} \times \nabla\psi$. Our Lagrangian rearrangement algorithm is only used to project the values onto an Eulerian frame when we want to view the solution (yellow branch). Notice that the error in rearrangement does not propagate to future time steps since we do not feed it back to the solution in the advection loop.

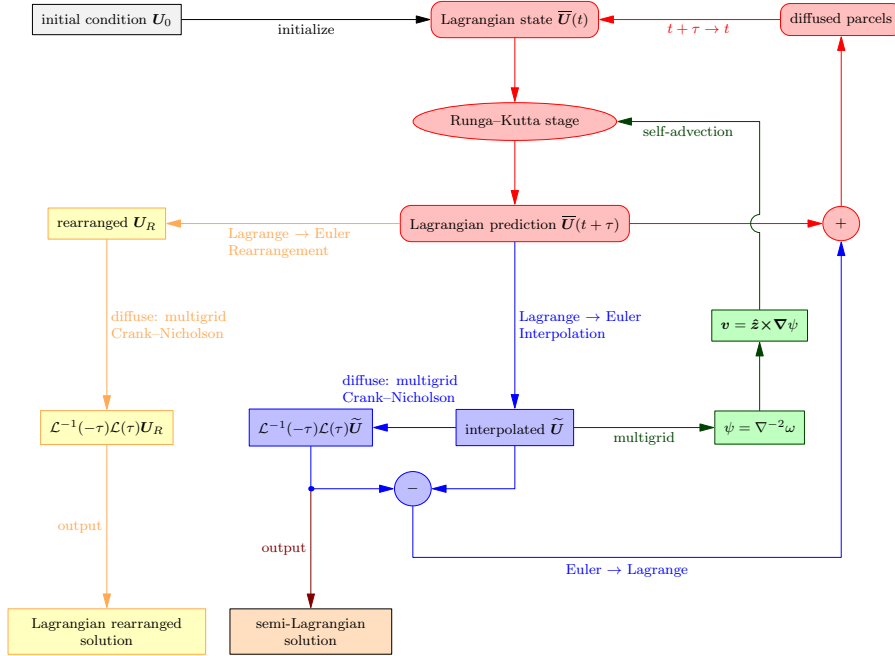


Fig. 5 Semi-Lagrangian and Lagrangian rearrangement schemes.

5 Complexity

A computer code in the C++ programming language was used to implement our Lagrangian rearrangement algorithm. For simplicity we consider a two-dimensional uniform lattice with $n = 2^{2m}$ grid points and doubly periodic boundary conditions, where m is a non-negative integer. The cost of running the code with respect to time, the *complexity*, is easily estimated as a function of n . Let us now establish that the computation time for the Lagrangian

```

for  $k = 1$  to  $n$  do
  Initialize parcels in Lagrangian buffer with local Eulerian position and  $\mathbf{U}$  values;
  Advect each parcel in the Lagrangian buffer via a Runge–Kutta stage;
  Compute area-weighted interpolated  $\tilde{\mathbf{U}}$  from the Lagrangian buffer;
  Compute updated advecting velocity  $\hat{\mathbf{z}} \times \nabla \nabla^{-2} \omega$ ;
  Compute diffusion contribution  $[\mathcal{L}^{-1}(-\tau)\mathcal{L}(\tau) - 1]\tilde{\mathbf{U}}$ ;
  Apply area-weighted diffusion contribution to each parcel in Lagrangian buffer;
  Copy the advected Lagrangian solution to the rearrangement buffer;
  Count the parcels in each cell of the rearrangement buffer;
  Push excess parcels from each pile to a nearby hole in the rearrangement buffer;
  Diffuse and output the rearranged Lagrangian solution:  $\mathcal{L}^{-1}(-\tau)\mathcal{L}(\tau)\mathbf{U}_R$ ;
end

```

Algorithm 1: Lagrangian rearrangement.

rearrangement algorithm scales linearly with n . The only places that must be focused on are the search for the nearest hole and the pushing of the parcels, procedures that must be repeated for many of the n cells. In computing the complexity of these parts of the algorithm, we concentrate on the *average complexity*, which computes the cost of an event while taking into account the probability of that event occurring (see [3]). First, assume that the entire grid is of unit size, so that the area of each cell is $1/n$. If a parcel is randomly assigned to a cell, the probability of a cell containing that parcel is $1/n$, and the probability that it does not is $1 - 1/n$. Using the binomial distribution, the probability of a cell containing k parcels is

$$P(k) \doteq \binom{n}{k} \left(\frac{1}{n}\right)^k \left(1 - \frac{1}{n}\right)^{n-k}.$$

Therefore, the probability of having a hole is $P(0) = (1 - 1/n)^n$, which approaches $1/e$ for n sufficiently large; the probability of not having a hole thus approaches $1 - 1/e$. For most numerical simulations the domain chosen is very large (in our test simulations n is typically set to 2^{18}).

For computing the cost of the search, one must calculate the probability of not finding a hole. In general, the goal is to start with a pile and search outward for the nearest hole in a shell-like domain. In Fig. 6, the cell labelled A is the pile, which is the center of the search, and the green ring is the first shell searched. Let $k = 1, 2, \dots$ denote the shell number being searched, as shown in Fig. 6. The number of cells searched so far, up to but not including shell k , will then be $4k(k - 1)$, and the number of cells in the k th shell is $8k$. The algorithm will reach shell index k if it does not find any holes up to index $k - 1$. Therefore, the probability of not having a hole in the first $k - 1$ shells is $(1 - 1/e)^{4k(k-1)}$, which is equivalent to the probability of searching $k - 1$ shells. Here, it is assumed that $4k(k - 1)$ is much smaller than n , so that the probability of not having a hole is independent of the number of parcels. Also, we assume that the probabilities of cells being or not being holes are independent of one another.

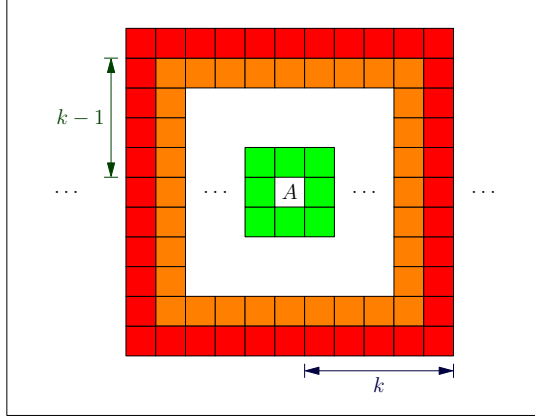


Fig. 6 Search order and shell index.

The final approximated *average searching cost* $A_s(n)$ will be the sum, over the entire domain, of the above probability multiplied by the number of cells in shell k , so the searching cost is given by

$$A_s(n) = \sum_{k=1}^{\sqrt{n}/2} 8k \left(1 - \frac{1}{e}\right)^{4k(k-1)},$$

which tends to a small constant (approximately 8.4) as n becomes large, meaning that the average cost of a single search grows insignificantly as the domain size gets bigger. This sum was evaluated numerically using the symbolic algebra program `Maple`. To calculate the cost of identifying the path, recall that if more than one hole is detected in a shell, the Bresenham algorithm is carried out for all such holes in that shell. Therefore, we must also consider the probability of finding more than one hole in the k th shell. We show in Theorem 1 (Appendix B) that at most $\lceil 1.82x \rceil$ steps are needed to find a path between a pile and a hole separated by a distance x . As in the above calculation of the searching cost, the probability of having to perform the Bresenham algorithm to find a path from a parcel to a cell in the k th shell is the same as the probability of not having a hole in the first $k-1$ shells, which is $(1 - 1/e)^{4k(k-1)}$. Moreover, the diagonal distance from the center of a search to a cell in the k th shell is at most $k\sqrt{2}$. Thus, the *average weighted Bresenham cost* $A_b(n)$ is 1.82 multiplied by the approximate probable distance from a pile to a hole times the expected number of holes in the first shell k that contains a hole (given by the conditional probability in Appendix C):

$$A_b(n) \approx 1.82 \sum_{k=1}^{\sqrt{n}/2} k\sqrt{2} \left(1 - \frac{1}{e}\right)^{4k(k-1)} 8k \left(\frac{1}{e}\right) \frac{1}{1 - (1 - \frac{1}{e})^{8k}}.$$

Using `Maple`, we found $A_b(n)$ tends to a small constant (approximately 8.6) as the domain gets larger. A path is now identified, and we must push the

parcels in this path. The actual pushing cost $A_p(n)$ is

$$A_p(n) = 1.82 \sum_{k=1}^{\sqrt{n}/2} k\sqrt{2} \left(1 - \frac{1}{e}\right)^{4k(k-1)}.$$

Again, using `Maple` we found $A_p(n)$ converges to a small constant (approximately 2.7) as the domain gets larger. In conclusion, the total complexity of the entire Lagrangian algorithm remains $O(n)$.

6 Results

An important feature of Lagrangian rearrangement is the conservation of Casimirs. In the absence of diffusion, any piecewise continuous function of the vorticity is conserved. For example, the concentration field must attain the same set of values at all time steps. To test this attribute thoroughly we have initially set the concentration at the n grid points to n distinct values. At each time step the code verifies, in the absence of diffusion, that exactly one cell contains each assigned value at all times; that is, the predicted configuration is simply a rearrangement of the initial condition, as illustrated for 16 grid points in Figure 1(b).

To demonstrate the parcel rearrangement property visually at higher resolutions, consider an initial concentration field that consists only of the values zero and one, which we display as black and white pixels, respectively. We self-consistently evolve a field consisting of a white horizontal band $y \in [0.25, 0.75]$ on a black background in the unit square $[0, 1] \times [0, 1]$, with semi-Lagrangian interpolation and Lagrangian rearrangement, using zero diffusion. The initial vorticity field is $\omega = -4\pi \sin(2\pi x) \cos(2\pi y)$, which corresponds to the velocity components $v_x = \sin(2\pi x) \cos(2\pi y)$ and $v_y = -\cos(2\pi x) \sin(2\pi y)$. We used a 512×512 grid, so that the grid scale is $h = 1.95 \times 10^{-3}$. The time step τ was chosen to be 10 times the Courant condition, or 1.95×10^{-2} units. We checked that the Lagrangian displacements computed by our fourth-order Runge–Kutta integration were sufficiently accurate at this large time step. The fact that one can run the algorithm at 10 times the Courant condition is an important advantage of Lagrangian schemes. A snapshot of the same advected stage predicted by the two methods is shown in Fig. 7. The left frame (a) shows the concentration field for the semi-Lagrangian method; the frame on the right (b) illustrates the predictions of Lagrangian rearrangement. With the selected palette, it is observed that the interpolation in the semi-Lagrangian method leads to coloured pixels, despite the absence of physical diffusion. This indicates that the method introduces spurious numerical diffusion, whereas Lagrangian rearrangement produces only black and white pixels, because there is no numerical diffusion.

Lagrangian rearrangement can also be applied to the full advection–diffusion equation. Using the same initial vorticity field as in the previous example, we consider a self-advected flow with diffusion constant $D = 2 \times 10^{-6}$. We

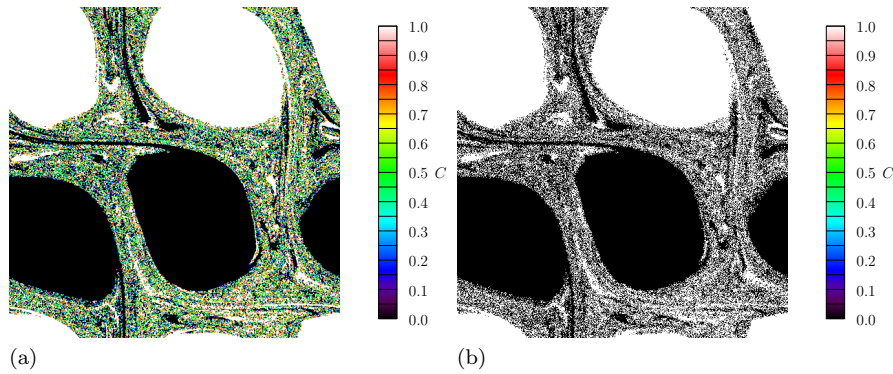


Fig. 7 Predictions after 750 time steps for advection in the absence of diffusion of a concentration field consisting of values 0 and 1 only for (a) semi-Lagrangian interpolation; (b) Lagrangian rearrangement.

compare the pushing method for viewing the Lagrangian data with area-weighted interpolated (semi-Lagrangian) projection. We initialized the runs with identical doubly periodic initial concentration fields (0 at the top and bottom varying gradually to 1 in the middle). Figures 8–10 demonstrate the advection and diffusion of this field by semi-Lagrangian interpolation and Lagrangian rearrangement. Although the two methods produce similar results, the solution in the interpolated results is seen to be smoother, due to the interpolation of concentration values by the semi-Lagrangian method. In contrast, the slight roughness at the pixel level exhibited in the Lagrangian rearranged results is a consequence both of lack of anomalous numerical diffusion and the inherent arbitrariness of our parcel-pushing algorithm.

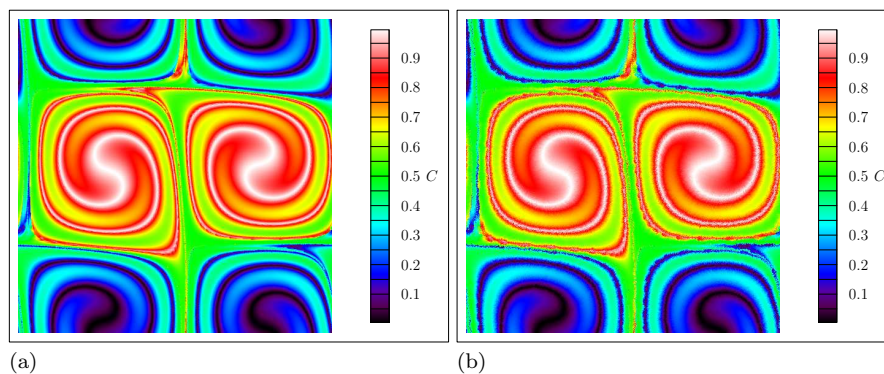


Fig. 8 Predictions after 100 time steps for the advection–diffusion of a smooth concentration field for (a) semi-Lagrangian interpolation; (b) Lagrangian rearrangement.

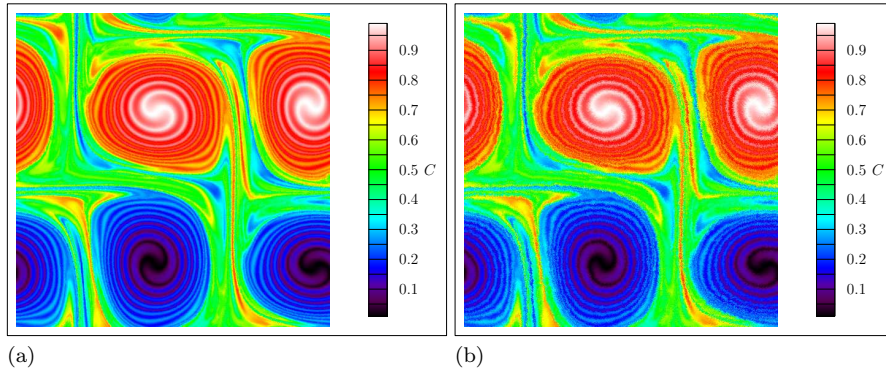


Fig. 9 Predictions after 500 time steps for the advection–diffusion of a smooth concentration field for (a) semi-Lagrangian interpolation; (b) Lagrangian rearrangement.

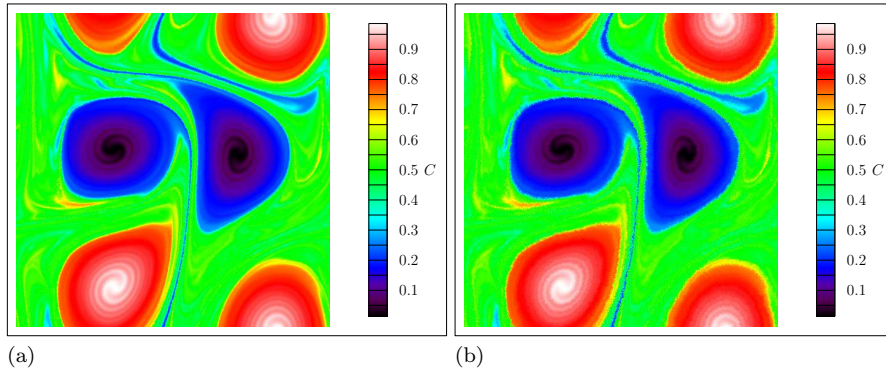


Fig. 10 Predictions after 1000 time steps for the advection–diffusion of a smooth concentration field for (a) semi-Lagrangian interpolation; (b) Lagrangian rearrangement.

We also applied Lagrangian rearrangement to Zalesak’s classic test for passive advection of a slotted disk [41,27]. Superimposing a 128×128 grid on the unit square, we advect a slotted disk centered at $(0.5, 0.75)$, having a radius of 15 cells and a slot width of 5 cells, with a passive velocity field $(\pi - 2\pi y, 2\pi x - \pi)$, using a time step of $1/628$. The Lagrangian-rearranged solution after 600 time steps is shown in Figure 11 (a). Although our rearrangement algorithm produces some artifacts in the output, the slotted disk retains its basic shape and is qualitatively similar to the flux-corrected transport (new limiter) solution in Fig. 13 of [41]. Most importantly, this error does not propagate to future time steps: after one complete rotation, the rearranged Lagrangian solution in Figure 11 (b) returns to a state indistinguishable from the initial condition.

The most important advantage of Lagrangian rearrangement over semi-Lagrangian methods is its conservation of Casimir invariants. In the absence of diffusion, the numerical approximation of the *concentration energy* $\frac{1}{2} \int C^2 d\mathbf{x}$

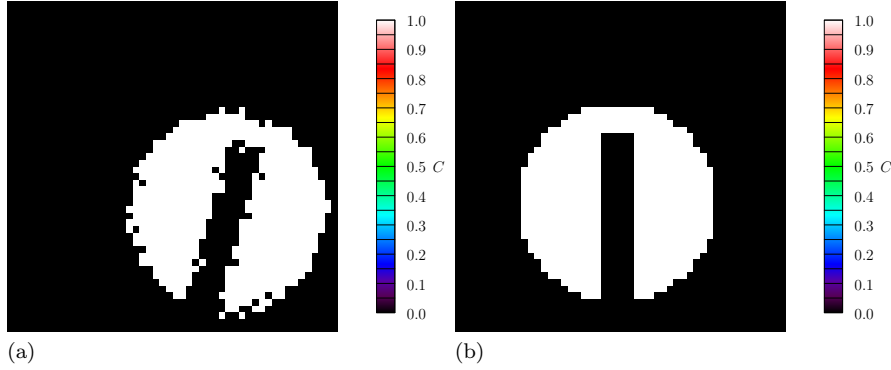


Fig. 11 Lagrangian rearrangement prediction for the Zalesak slotted disk: (a) after 600 time steps; (b) after one complete rotation (628 time steps). Only a portion of the 128×128 domain is shown.

and the *enstrophy* $Z = \frac{1}{2} \int \omega^2 d\mathbf{x}$ should be conserved. In Figs. 12 and 13 it is observed that Lagrangian rearrangement indeed respects the invariance of these two important quantities. On the other hand, in the semi-Lagrangian method both of these quantities decay as a result of unwanted numerical diffusion. Moreover, in the presence of diffusion one can consider the energy equation obtained by multiplying both sides of (8) by \mathbf{U} and integrating over the domain. On integrating by parts and invoking the incompressibility condition and doubly periodic boundary conditions, one finds that the concentration energy fields should decay as

$$\frac{1}{2} \frac{\partial}{\partial t} \int C^2 d\mathbf{x} = -D \int |\nabla C|^2 d\mathbf{x}. \quad (10)$$

It is convenient to introduce the normalized energy decay rates

$$\frac{\frac{\partial}{\partial t} \int C^2 d\mathbf{x}}{\int C^2 d\mathbf{x}} \quad \text{and} \quad \frac{-2D \int |\nabla C|^2 d\mathbf{x}}{\int C^2 d\mathbf{x}}. \quad (11)$$

Analogous quantities for the enstrophy decay rate, obtained by replacing C by the scalar vorticity ω , are also of interest.

According to (10), the energy decay rates for each field, as calculated by the two corresponding expressions, should agree. The values in (11) for both semi-Lagrangian interpolation and Lagrangian rearrangement are plotted in Fig. 14 (and in Fig. 15 for the ω field). As seen in the graphs, the decay rates predicted by the semi-Lagrangian method (denoted by the subscript I) do not agree, whereas the rates for the rearranged Lagrangian solution (denoted by the subscript R) agree much better, to within the expected spatial discretization error. The anomalous and erratic numerical diffusion exhibited by the semi-Lagrangian solution is evident both in the departure of the blue and green

curves and in the suppression of the energy content of ∇C_I relative to the other predictions. This shows that the term $\mathbf{v} \cdot \nabla U$ is not modelled by the semi-Lagrangian method to respect the correct energy decay rate for a real fluid.

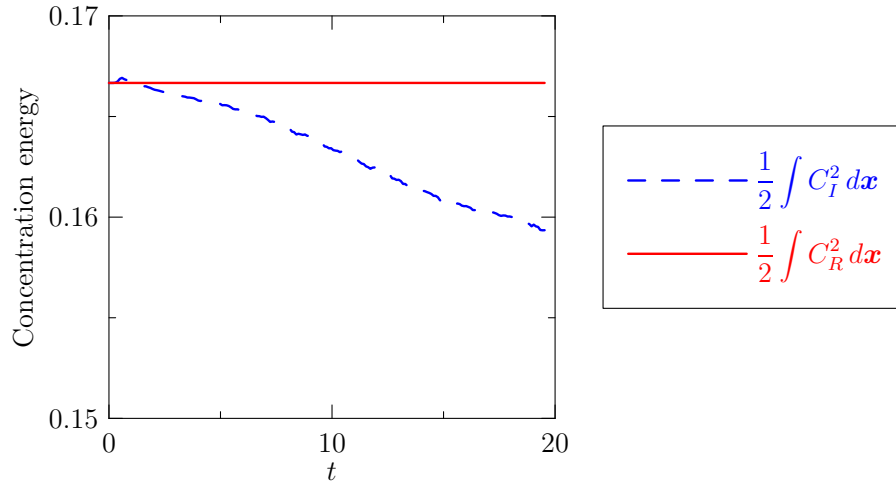


Fig. 12 Evolution of the concentration field energy predicted by the semi-Lagrangian (I) and rearrangement (R) methods when $\nu = D = 0$.

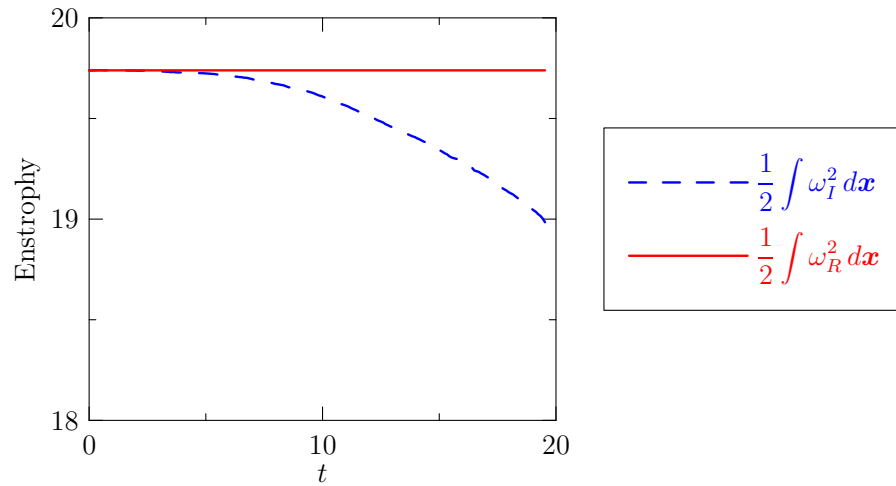


Fig. 13 Evolution of the enstrophy predicted by the semi-Lagrangian (I) and rearrangement (R) methods when $\nu = D = 0$.

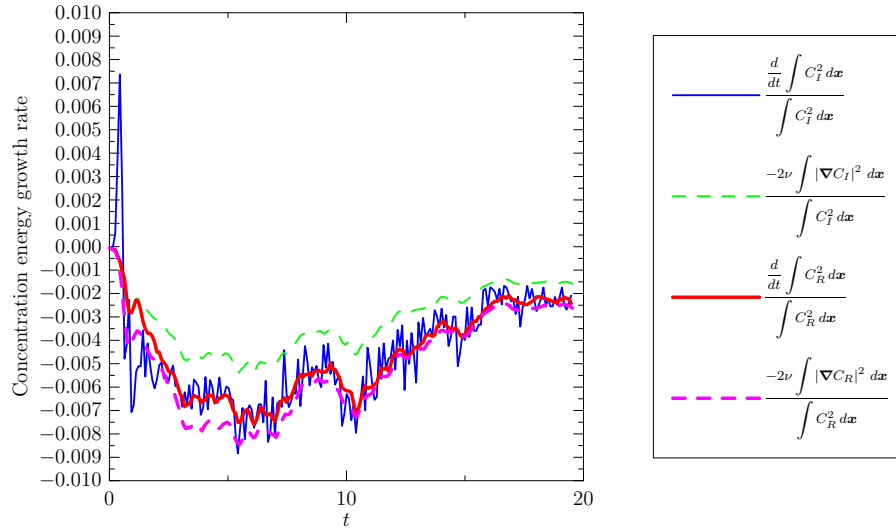


Fig. 14 Energy decay rates for the concentration field predicted by the semi-Lagrangian (*I*) and rearrangement (*R*) methods in the presence of diffusion.

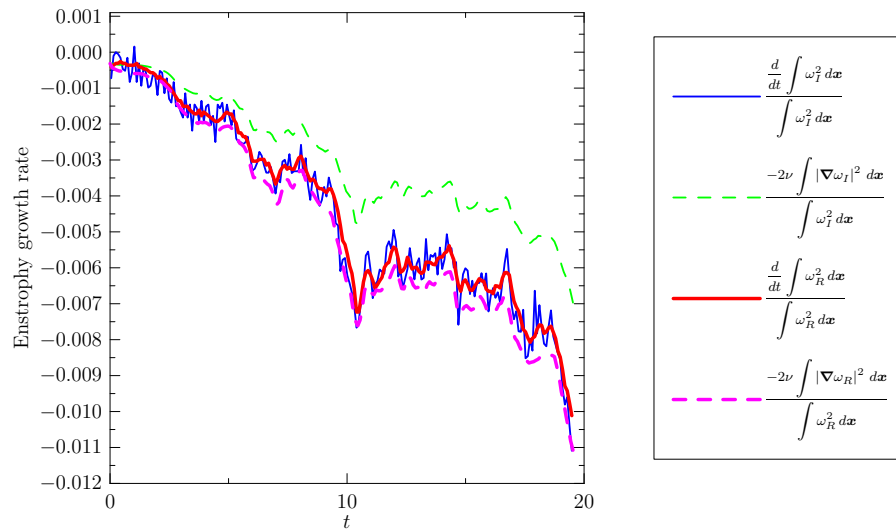


Fig. 15 Enstrophy decay rates predicted by the Lagrangian semi-Lagrangian (*I*) and rearrangement (*R*) methods in the presence of diffusion.

7 Conclusion

We propose a new fully Lagrangian method for solving advection equations. This method preserves Casimir invariants, just as inviscid fluids do. We argue in the nondiffusive case that the discretized values of the concentration field,

when viewed on an Eulerian grid, should only be rearranged, not changed, to enforce a discretized version of the Casimir invariance property of the nonlinear advection term. That is, the pixels that are ultimately used to visualize the flow should be treated as infinitesimal parcels: at all times, the generated concentration field should be some rearrangement of its initial state. The velocity field is used to advect the values of the concentration and vorticity field in the Lagrangian frame. In projecting the Lagrangian solution to an Eulerian frame, some of the cells (holes) will have no corresponding Lagrangian value, and some of the cells (piles) will have more than one value. In order to find the best projection from Lagrangian to Eulerian coordinates, we determine a path from a pile to the nearest hole and push the chain of parcels (values) towards the hole. This path is calculated using a weighted version of the Bresenham algorithm for drawing digitized lines. This modified version reduces the error in pushing parcels away from their calculated Lagrangian position: the weight used is the distance between the parcel and its position is determined by Lagrangian advection. The weighted version attempts to choose a path containing parcels with minimal weight. To prevent the error in parcel pushing from propagating to the next time step, we do not reuse this information in future time steps. Lagrangian rearrangement thus merely provides an energy-respecting (and Casimir-respecting) filter for viewing the current Lagrangian solution in an Eulerian frame. To deal with self-advection, we interpolate the advected Lagrangian vorticity field onto the Eulerian grid, avoiding any pushing error from being transmitted to the velocity field. We then calculate the new velocity from the projected vorticity by inverting a Laplacian with a multigrid solver.

In summary, the method of Lagrangian rearrangement can be used to view Lagrangian solutions of passive and self-consistent advection, avoiding the introduction of any artificial numerical diffusion. More importantly, for scientific applications, we have shown how operator splitting can be used to account for the effects of physical diffusion in a manner that yields better concentration energy decay characteristics than straightforward Lagrangian interpolation.

In future work, it would be interesting to explore the idea of advecting parcel vertices rather than their centroids. Even if an area-preserving correction was implemented, however, one will likely encounter difficulties with degenerate parcels that have been highly elongated by the advecting flow. It would also be interesting to explore some kind of entropic (or total variation diminishing) process to minimize the oscillations inherent in our somewhat arbitrary parcel pushing process. Ideally, after each time step, one would like to identify a point on the rearrangement manifold that is closest (say in the L_2 norm) to the predicted Lagrangian output. In practice the full minimization problem is very costly to solve in real time. The weighted Bresenham scheme we have proposed is a practical and efficient first approximation towards this goal, motivated by the tendency of fluids to seek the path of least resistance. We hope that the demonstration of Lagrangian rearrangement will inspire others

to develop efficient quasi-minimization techniques that lead to improved parcel rearrangement.

A Weighted Bresenham Algorithm

In our weighted version of the Bresenham algorithm, the choice of the next point in the path depends on the weight of the eligible neighbouring cells. Fig. 16 shows eight cases depending on the location of the destination point. One seeks a neighbouring cell in the general direction of the path with the lowest weight. If the slope is zero, the cells to the north-east, east, and south-east of the current cell are searched. The north-east and east cells are searched if the slope is between zero and one, the north, north-east, and east cells are searched if the slope is one, and the north and north-east cells are searched if the slope is greater than one. If the slope is infinity, the cells to the north-west, north, and north-east of the current cell are searched. Should the weight of two or more cells be the same, the original Bresenham algorithm will be the tie-breaker. The following is `Asymptote` code (a vector graphics language for technical drawing [22, 7]), along with eight sample output paths, for our weighted Bresenham algorithm (optimized so that all cases are mapped to the first quadrant).

```
pair[] discreteline(int x, int y, int x2, int y2, int[][] count)
{
  pair[] line;
  while(true) {
    int signx,signy;
    int dx=x2-x, dy=y2-y;
    if(dx < 0) {
      signx=-1; dx=-dx;
    } else signx=1;
    if(dy < 0) {
      signy=-1; dy=-dy;
    } else signy=1;
    line.push((x,y));
    if(dx >= dy) {
      if(dx <= 1) {
        if(dx > 0) line.push((x2,y2));
        return line;
      }
      int N=count[x][y+signy];
      int NE=count[x+signx][y+signy];
      int E=count[x+signx][y];
      if(dx == dy) {
        if(E >= NE && E >= N) { // NE or N
          y += signy;
          if(NE <= N) x += signx; // favour NE
        } else if(N >= NE && N >= E) { // NE or E
          x += signx;
          if(NE <= E) y += signy; // favour NE
        } else { // E or N
          if(E <= N) x += signx; // favour E
          else y += signy;
        }
      } else {
        int SE=count[x+signx][y-signy];
        x += signx;
        if(dy == 0) {
          if(SE >= E && SE >= NE) { // E or NE
```

```

        if(NE < E) y += signy;           // favour E
    } else if(NE >= E && NE >= SE) {    // E or SE
        if(SE < E) y -= signy;         // favour E
    } else {                             // NE or SE
        if(NE <= SE) y += signy;       // favour NE
        else y -= signy;
    }
    } else if(NE < E || (NE == E && dx <= 0)) // E or NE
        y += signy;                     // favour Bresenham
    }
} else {
    if(dy == 1) {
        line.push((x2,y2));
        return line;
    }
    int N=count[x][y+signy];
    int NE=count[x+signx][y+signy];
    int NW=count[x-signx][y+signy];
    y += signy;
    if(dx == 0) {
        if(NW >= N && NW >= NE) {      // N or NE
            if(NE < N) x += signx;     // favour N
        } else if(NE >= N && NE >= NW) { // N or NW
            if(NW < N) x -= signx;     // favour N
        } else {                       // NE or NW
            if(NE <= NW) x += signx;   // favour NE
            else x -= signx;
        }
    } else if(NE < N || (NE == N && dy <= 0)) // N or NE
        x += signx;                     // favour Bresenham
    }
}
return line;
}

```

B Termination of Weighted Bresenham Algorithm

Theorem 1 (Termination of weighted Bresenham) *The weighted Bresenham algorithm produces a finite path between any two points on a regular lattice. For a unit square lattice, at most $\lceil 1.82x \rceil$ steps are needed to connect two points that are a distance x apart.*

Proof Let A and B be given on the grid. We want to find the desired path between them. For simplicity, we assume that B is inside or on the boundary of the first octant with respect to A . Without loss of generality, consider a unit square lattice. As described before, depending on the position of B , we have either two or three choices for the next cell to be included in the path. If one of these choices is the grid point B , we are done; the algorithm terminates after choosing B . Otherwise, in choosing one of the immediate neighbours of the current cell, we will take a step of size 1 or $\sqrt{2}$. We must show that there exists a fixed number $\delta > 0$ such that the distance to the point B in each step is always reduced by at least δ . The algorithm will then terminate in a finite number of steps.

Case (i): Assume B lies on the same horizontal line as A , so that the slope of the line from A to B is zero, ($m = 0$). In this case (Fig. 17), the next point in the path is one of the points C , D , or F . If we choose D , then since $\overline{DB} = \overline{AB} - 1$, a step of 1 is taken toward B . Suppose instead that we choose C . On letting $x = \overline{AB} \geq 2$ and $\delta = x - \overline{CB} = 1 + \overline{DB} - \overline{CB} < 1$

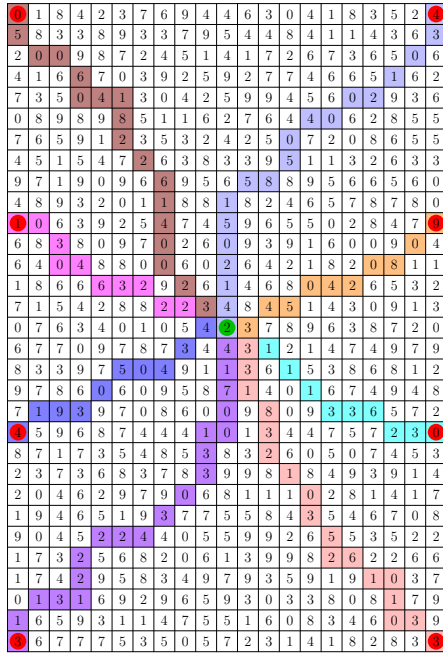


Fig. 16 Paths of local minimal weight from the center circle to eight edge circles, as determined by the weighted Bresenham algorithm and the indicated numerical parcel weights.

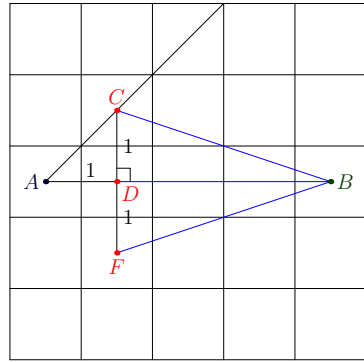


Fig. 17 Case(i): $m = 0$.

(since $\overline{DB} < \overline{CB}$), and noting that $\delta = \overline{AD} + \overline{DB} - \overline{CB} = \overline{CD} + \overline{DB} - \overline{CB} > 0$, we find that

$$(x - \delta)^2 = \overline{CB}^2 = \overline{DB}^2 + 1 = (\overline{AB} - 1)^2 + 1 = \overline{AB}^2 - 2\overline{AB} + 2 = x^2 - 2x + 2,$$

so that $-2x\delta + \delta^2 = -2x + 2$. We then deduce from $x \geq 2$ that $2 - \delta^2 = 2x(1 - \delta) \geq 4(1 - \delta)$. Thus $\delta^2 - 4\delta + 2 \leq 0 \implies \delta \in [2 - \sqrt{2}, 1)$. The same argument of course also holds for the choice F . The distance reduction in this case is thus at least $2 - \sqrt{2}$.

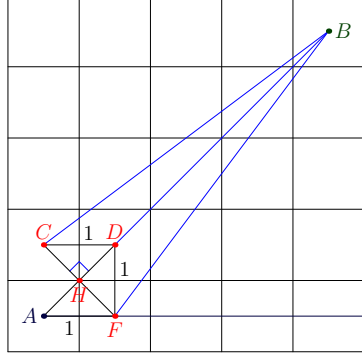


Fig. 18 Case(ii): $m = 1$.

Case (ii): Assume that the slope of the line from A to B is 1. In this case (Fig. 18), the next point in the path will be one of the points C , D , or F . Here $\overline{AB} = \overline{DB} - \sqrt{2}$. If we choose D , we take a step of size $\sqrt{2}$ toward B . Suppose instead that we choose C . We see that $\overline{CH} = \overline{AH} = 1/\sqrt{2}$. On letting $x = \overline{AB}$, we obtain

$$(x - \delta)^2 = \overline{CB}^2 = \overline{HB}^2 + \overline{CH}^2 = \left(x - \frac{1}{\sqrt{2}}\right)^2 + \frac{1}{2} = x^2 - \sqrt{2}x + 1.$$

Thus $-2x\delta + \delta^2 = -\sqrt{2}x + 1$. We know that $x \geq 2\sqrt{2}$ since B is not one of the choices, so $\delta^2 - 1 = x(2\delta - \sqrt{2}) \geq 2\sqrt{2}(2\delta - \sqrt{2}) = 4\sqrt{2}\delta - 4$. Now $\delta^2 - 4\sqrt{2}\delta + 3 \leq 0 \implies \delta \geq 2\sqrt{2} - \sqrt{5}$. The same argument of course also holds for the choice F . The distance reduction in this case is thus at least $2\sqrt{2} - \sqrt{5}$.

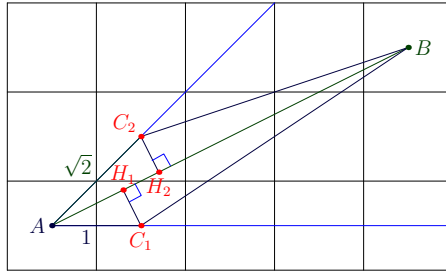


Fig. 19 Case(iii): $0 < m < 1$.

Case (iii): Assume B lies inside the first octant ($0 < m < 1$). In this case, Fig. 19, the next point in the path is one of the two points C_1 or C_2 . Let $x = \overline{AB}$. Notice that $x \geq \sqrt{5}$ since B is not one of the points C_1 or C_2 . Let C be the point (C_1 or C_2) that is selected, drop the perpendicular \overline{CH} to \overline{AB} . Let $y = \overline{CB}$ and $z = \overline{AC}$ and note that $z = 1$ if $C = C_1$

and $z = \sqrt{2}$ if $C = C_2$. Since $0 < \angle CAH < \pi/4$, we know that $\overline{AH}/z > 1/\sqrt{2}$. On letting $\delta = x - \overline{CB}$, we find that

$$\begin{aligned} (x - \delta)^2 &= \overline{CB}^2 = \overline{HB}^2 + \overline{CH}^2 = (\overline{AB} - \overline{AH})^2 + \overline{AC}^2 - \overline{AH}^2 \\ &= x^2 - 2x\overline{AH} + z^2 < x^2 - 2x\frac{z}{\sqrt{2}} + z^2. \end{aligned}$$

Thus $-2x\delta + \delta^2 < -\sqrt{2}xz + z^2$, so that $z^2 - \delta^2 > x(\sqrt{2}z - 2\delta) \geq \sqrt{5}(\sqrt{2}z - 2\delta)$. Hence, $\delta^2 - 2\sqrt{5}\delta + \sqrt{10}z - z^2 < 0$. For $z = 1$ this implies that $\delta > \sqrt{5} - \sqrt{6 - \sqrt{10}}$ and for $z = \sqrt{2}$ this implies that $\delta > \sqrt{5} - \sqrt{7 - 2\sqrt{5}}$.

In all cases, the distance between the point B and the new included point is thus always less than \overline{AB} by an amount

$$\begin{aligned} \delta &= \min \left\{ 1, \sqrt{2}, 2 - \sqrt{2}, 2\sqrt{2} - \sqrt{5}, \sqrt{5} - \sqrt{6 - \sqrt{10}}, \sqrt{5} - \sqrt{7 - 2\sqrt{5}} \right\} \\ &= \sqrt{5} - \sqrt{6 - \sqrt{10}} > 0.551. \end{aligned}$$

That is, at most $\lceil 1.82\overline{AB} \rceil$ steps will be required to reach the point B .

C Multiple-Hole Expected Value

The expected number of holes in a shell k (with $8k$ cells) containing a hole is

$$\langle j \rangle = \frac{\sum_{j=1}^{8k} j \binom{8k}{j} \left(1 - \frac{1}{e}\right)^{8k-j} \left(\frac{1}{e}\right)^j}{\sum_{j=1}^{8k} \binom{8k}{j} \left(1 - \frac{1}{e}\right)^{8k-j} \left(\frac{1}{e}\right)^j} = \frac{\sum_{j=1}^{8k} j \binom{8k}{j} r^j}{\sum_{j=1}^{8k} \binom{8k}{j} r^j},$$

where $r = 1/(e - 1)$. Since the probability of not having a hole in $8k$ cells is $(1 - 1/e)^{8k}$, we get

$$\sum_{j=1}^{8k} \binom{8k}{j} \left(1 - \frac{1}{e}\right)^{8k-j} \left(\frac{1}{e}\right)^j = 1 - \left(1 - \frac{1}{e}\right)^{8k},$$

which on multiplying both sides by $(r + 1)^{8k} = (1 - 1/e)^{-8k}$, can be written as

$$\sum_{j=1}^{8k} \binom{8k}{j} r^j = (r + 1)^{8k} - 1.$$

On differentiating both sides with respect to r and then multiplying by r , it follows that

$$\sum_{j=1}^{8k} \binom{8k}{j} j r^j = 8kr(r + 1)^{8k-1}.$$

The expected number of holes thus evaluates to

$$\langle j \rangle = \frac{8kr(r + 1)^{8k-1}}{(r + 1)^{8k} - 1} = \frac{8k \left(1 - \frac{1}{r + 1}\right)}{1 - \left(1 - \frac{1}{r + 1}\right)^{8k}} = \frac{8k \left(\frac{1}{e}\right)}{1 - \left(1 - \frac{1}{e}\right)^{8k}}.$$

This of course is just the probability $1/e$ of finding a hole times the number of holes, conditioned on the probability that the shell contains at least one hole.

References

1. Alam, J., Bowman, J.: Energy-conserving simulation of incompressible electro-osmotic and pressure-driven flow. *Theoretical and Computational Fluid Dynamics* **16**, 1–18 (2002)
2. Ames, W.: *Numerical Methods for Partial Differential Equations*. Academic Press, San Diego, CA (1977)
3. Basse, S., Gelder, A.V.: *Computer Algorithms, Introduction to Design and Analysis*. Addison-Wesley, Ontario (2000)
4. Behrens, M.: A conservative scheme for 2D and 3D adaptive semi-Lagrangian advection. In: Z.C. Shi, Z. Chen, T. Tang, D. Yu (eds.) *Recent Advances in Adaptive Computation*, vol. 383, pp. 219–234. American Mathematical Society, Providence, Rhode Island (2005)
5. Behrens, J.: A parallel adaptive finite-element semi-Lagrangian advection scheme for the shallow water equations. In: *Modeling and Computation in Environmental Sciences, Proceedings of the First GAMM-Seminar at ICA Stuttgart, Notes on Numerical Fluid Mechanics*, vol. 59, pp. 49–60. Vieweg, Braunschweig (1997)
6. Bowman, J.C.: Casimir cascades in two-dimensional turbulence. *J. Fluid Mech* **729**, 364–376 (2013)
7. Bowman, J.C., Hammerlindl, A.: Asymptote: A vector graphics language. *TUGboat: The Communications of the T_EX Users Group* **29**(2), 288–294 (2008)
8. Bramble, J.H.: *Multigrid Methods*. Longman Scientific and Technical, London (1993)
9. Bresenham, J.E.: Algorithm for computer control of a digital plotter. *IBM Systems Journal* **4**, 25–30 (1965)
10. Courant, R., Friedrichs, K., Lewy, H.: On the partial differential equations of mathematical physics. *IBM Journal of Research and Development* **11**, 215–234 (1967)
11. Crabtree, H.J., Cheong, E.C., Tilroe, D.A., Backhouse, C.J.: Microchip injection and separation anomalies due to pressure effects. *Analytical chemistry* **73**(17), 4079–4086 (2001)
12. Dritschel, D.G.: Contour surgery: a topological reconnection scheme for extended integrations using contour dynamics. *Journal of Computational Physics* **77**(1), 240–266 (1988)
13. Dritschel, D.G., Ambaum, M.H.: A contour-advective semi-lagrangian numerical algorithm for simulating fine-scale conservative dynamical fields. *Quarterly Journal of the Royal Meteorological Society* **123**(540), 1097–1130 (1997)
14. Eyink, G.L.: Exact results on stationary turbulence in 2D: consequences of vorticity. *Physica D* **91**, 97–142 (1996)
15. Falkovich, G., Hanany, A.: Is 2D turbulence a conformal turbulence? *Phys. Rev. Lett.* **71**, 3454–3457 (1993). DOI 10.1103/PhysRevLett.71.3454. URL <http://link.aps.org/doi/10.1103/PhysRevLett.71.3454>
16. Fraccarollo, L., Capart, H., Zech, Y.: A Godunov method for the computation of erosional shallow water transients. *International Journal For Numerical Methods In Fluids* **41**, 951–976 (2003)
17. Gingold, R.A., Monaghan, J.J.: Smoothed particle hydrodynamics-theory and application to non-spherical stars. *Monthly notices of the royal astronomical society* **181**, 375–389 (1977)
18. Godunov, S.: A finite difference method for the numerical computation of discontinuous solutions of the equations of fluid dynamics. *Sbornik. Mathematics* **47**, 271–290 (1959)
19. Gremaud, P.A., Kuster, C.M., Li, Z.: A study of numerical methods for the level set approach. *Applied numerical mathematics* **57**(5), 837–846 (2007)
20. Grigoryev, Y., Vshivkov, V., Fedoruk, M.: *Numerical “Particle-in-Cell” Methods—theory and applications*. Brill Academic Publishers, Utrecht-Boston (2002)
21. Hackbusch, W.: *Multi-Grid Methods and Applications*. Series in Computational Mathematics. Springer, New York (1985)
22. Hammerlindl, A., Bowman, J.C., Prince, R.T.: *Asymptote: a descriptive vector graphics language* (2004). Available online at <http://asymptote.sourceforge.net>
23. Kees, C.E., Akkerman, I., Farthing, M.W., Bazilevs, Y.: A conservative level set method suitable for variable-order approximations and unstructured meshes. *Journal of Computational Physics* **230**(12), 4536–4558 (2011)

24. Lax, P., Wendroff, B.: System of conservation laws. *Communications on Pure and Applied Mathematics* **13**, 217–237 (1960)
25. Leboeuf, J., Tajima, T., Dawson, J.: Magnetohydrodynamics particle code for fluid simulation of plasmas. *Journal of Computational Physics* **31**, 379–408 (1979)
26. Leslie, L.M., Purser, R.J.: Three-dimensional mass-conserving semi-Lagrangian scheme employing forward trajectories. *Monthly Weather Review* **123**(8), 25 (1995)
27. Marchandise, E., Remacle, J.F., Chevaugeon, N.: A quadrature-free discontinuous galerkin method for the level set equation. *Journal of Computational Physics* **212**(1), 338–357 (2006)
28. Morrison, P.J.: Hamiltonian description of the ideal fluid. *Rev. Mod. Phys.* **70**, 467–521 (1998)
29. Osher, S., Sethian, J.A.: Fronts propagating with curvature-dependent speed: algorithms based on hamilton-jacobi formulations. *Journal of computational physics* **79**(1), 12–49 (1988)
30. Polyakov, A.: The theory of turbulence in two dimensions. *Nuclear Physics B* **396**, 367 – 385 (1993). DOI 10.1016/0550-3213(93)90656-A
31. Press, W.H., Teukolsky, S.A., Vetterling, W.T., Flannery, B.P.: *Numerical Recipes, The Art of Scientific Computing*, 2nd edn. Cambridge Univ. Press, Cambridge (1992)
32. Rothstein, D.M., Lovelace, R.V.: Advection of magnetic fields in accretion disks: not so difficult after all. *The Astrophysical Journal* **677**(2), 1221 (2008)
33. Sheu, T.W., Yu, C.: Numerical simulation of free surface by an area-preserving level set method. *Communications in Computational Physics* **11**(4), 1347 (2012)
34. Solenthaler, B., Pajarola, R.: Predictive-corrective incompressible sph. In: *ACM transactions on graphics (TOG)*, vol. 28, p. 40. ACM (2009)
35. Wang, H., Skamarock, W.C., Feingold, G.: Evaluation of scalar advection schemes in the advanced research wrf model using large-eddy simulations of aerosol–cloud interactions. *Monthly Weather Review* **137**(8) (2009)
36. Wang, Y., Hutter, K.: Comparisons of numerical methods with respect to convectively-dominated problems. *International Journal for Numerical Methods in Fluids* **37**, 721–745 (2001)
37. Woodward, P., Colella, P.: The numerical simulation of two-dimensional fluid flow with strong shocks. *Journal of Computational Physics* **54**, 115–173 (1984)
38. Woodward, P., Colella, P.: The piecewise parabolic method (ppm) for gas-dynamical simulations. *Journal of Computational Physics* **54**, 174–201 (1984)
39. Yong, Z., Benson, D.A., Meerschaert, M.M., Scheffler, H.P.: On using random walks to solve the space-fractional advection-dispersion equations. *Journal of Statistical Physics* **123**(1), 89–110 (2006)
40. Zabusky, N.J., Hughes, M., Roberts, K.: Contour dynamics for the euler equations in two dimensions. *Journal of computational physics* **30**(1), 96–106 (1979)
41. Zalesak, S.T.: Fully multidimensional flux-corrected transport algorithms for fluids. *Journal of computational physics* **31**(3), 335–362 (1979)
42. Zhuang, P., Liu, F., Anh, V., Turner, I.: Numerical methods for the variable-order fractional advection-diffusion equation with a nonlinear source term. *SIAM Journal on Numerical Analysis* **47**(3), 1760–1781 (2009)